



3

5

6

8

10

11

12

13

15

16

17

18

19

20

21

22

23

25

26

27

28

29

30

31

32

33

34

35

36

37

39

40

41

42

43

Article

Conserved structure associated with different 3'CITEs is important for translation of umbraviruses

Sayanta Bera, Muhammad Ilyas, Anna A. Mikkelsen, and Anne E. Simon*

Department of Cell Biology and Molecular Genetics, University of Maryland, College Park, MD, 20772, USA sbera@umd.edu (S.B.); milyassarwar@gmail.com (M.I.); amikkels@umd.edu (A.A.M)

Abstract: Cap-independent translation of plus-strand RNA plant viruses frequently depends on 3' structures to attract translation initiation factors that bind ribosomal subunits or bind directly to ribosomes. Umbraviruses are excellent models for studying 3' cap-independent translation enhancers (3'CITEs), as umbraviruses can have different 3'CITEs in the central region of their lengthy 3'UTRs, and also contain a particular 3'CITE (the T-shaped structure or 3'TSS) near their 3' ends. We discovered a novel hairpin just upstream of the centrally located (known or putative) 3'CITEs in all 14 umbraviruses. These CITE-associated structures (CAS) have conserved sequences in their apical loops and at the stem base and adjacent positions. In 11 umbraviruses, CAS are preceded by two small hairpins joined by a putative kissing-loop interaction (KL). Mutations in the CAS apical loop in opium poppy mosaic virus (OPMV) and pea enation mosaic virus 2 (PEMV2) enhanced translation of genomic (g)RNA, but not subgenomic (sg)RNA reporter constructs, and significantly repressed virus accumulation in Nicotiana benthamiana. Other mutations throughout OPMV CAS also repressed virus accumulation and enhanced sgRNA reporter translation, while mutations in the lower stem repressed gRNA reporter translation. Similar mutations in the PEMV2 CAS also repressed accumulation but did not significantly affect gRNA or sgRNA reporter translation with the exception of deletion of the entire hairpin, which only reduced translation of the gRNA reporter. OPMV CAS mutations had little effect on the downstream BTE 3'CITE or upstream KL element while PEMV2 CAS mutations significantly altered KL structures. These results introduce an additional element associated with cap-independent translation that differentially affects the structure and translation of different umbraviruses.

Keywords: Umbravirus; 3'CITE; BTE; cap-independent translation; SHAPE structure probing

1. Introduction

Unlike eukaryotic mRNAs that nearly invariantly contain a 5' m7GpppN cap and a 3' poly-A tail for efficient translation, plus-strand (+)RNA virus genomes translated in eukaryotic cells frequently require non-canonical mechanisms to outcompete cellular translation or to allow for translation when cap-dependent translation is suppressed [1,2]. Non-canonical translation frequently requires specific structures at the 5' and/or 3' ends of the genome to attract the translational machinery in the absence of a 5' cap. For (+)RNA viruses infecting plants, two types of *cis*-structures/elements have been identified that support cap-independent translation; internal ribosome entry sites (IRES), which are more commonly found in animal viruses, and 3' cap-independent translation enhancers (3'CITEs). Plant virus IRES are normally located either near the 5' end of the virus genome or proximal to internal ORFs, and can either be large complex structures as found in potyvirus triticum mosaic virus, or simple structures as found in turnip mosaic virus [3–5]. IRES can also be unstructured, non-specific sequences such as the turnip crinkle virus

Citation: To be added by editorial staff during production.

Academic Editor: Firstname Last-

Received: date Accepted: date Published: date

Publisher's Note: MDPI stays neutral with regard to jurisdictional claims in published maps and institutional affiliations.



Copyright: © 2022 by the authors. Submitted for possible open access publication under the terms and conditions of the Creative Commons Attribution (CC BY) license (https://creativecommons.org/licenses/by/4.0/).

^{*} Correspondence: simona@umd.edu

46

47

48

49

51

53

54

55

56

57

58

60

61

62

63

65

66

67

68

69

70

71

72

73

74

75

76

77

78

79

80

81

83

84

86

88

90

91

92

93

94

95

96

97

(TCV) IRES upstream of the 3'-proximal coat protein ORF [6]. Plant virus IRES are larger and generally more complex than the short, A-rich IRES that are in cellular mRNAs mediating immune response against pathogens when biotic stress inhibits canonical translation [7].

3'CITEs are located either within the viral 3'UTR or can extend into the upstream ORF [1]. First identified in satellite tobacco necrosis virus, 3'CITEs facilitate viral RNA translation from the 5' end of the genomic (g)RNA or subgenomic (sg)RNA by binding to eukaryotic translation initiation factors (eIFs) that subsequently recruit ribosomal subunits, or by binding directly to ribosomal subunits [1,8]. The initiation complex, which assembles at the 3' end of the viral genome, must be transferred to the 5' end, which is usually accomplished by a long-distance RNA:RNA interaction involving an unpaired sequence within the 3'CITE and an unpaired sequence at or near the 5' end [8,9]. Using *in vitro* translation assays, the long-distance interaction was found to enhance the number of templates translated and not the rate of initiation or the number of ribosomes occupying the template [10]. Using high-throughput bi-cistronic translation assays, 3'CITEs have also been identified in human RNA viruses and cellular mRNAs, highlighting their conservation and importance [11].

Plant virus 3'CITEs have been organized into at least eight distinct classes, based on conserved sequences and secondary structure, and their ability to interact with specific translation factors [1]. 3'CITEs appear to be modular units that have exchanged between viruses and then evolved independently, optimizing their functions according to the host-virus environment. Evidence for modular 3'CITEs was first reported for melon necrotic spot virus (MNSV; family *Tombusviridae*), which gained a second 3'CITE through recombination with an unrelated virus, thus allowing MNSV to bypass host resistance associated with the original CITE [12–14]. In addition, members of a single genus (e.g., carmovirus and umbravirus) can have different 3'CITEs occupying near identical locations [1].

Among the best characterized 3'CITEs are the barley yellow dwarf virus-like translation element (BTE) [8,15], the panicum mosaic virus-like translational enhancer (PTE) [16,17], and the T-shaped structure (TSS) that was first identified in carmoviruses [18]. BTEs are characterized by a signature 17-nt motif that forms a short stem-loop (SL) implicated (with other sequences) in the binding of eukaryotic initiation factor (eIF)4G. BTEs, which have been found in members of several genera within the Tombusviridae, were recently divided into three subclasses based on the number of apical SLs (at least two) and other conserved sub-class-specific features and motifs [8]. The PTE 3'CITE contains a Yshaped secondary structure composed of a three-way junction with two upper SLs, a supporting stem of 6 to 7 bp, a large G-rich asymmetric loop, and a lower supporting stem of different sizes [1]. The G-rich sequence forms a critical pseudoknot (PK) with C-rich sequence between the two SLs and is implicated in the binding of eIF4E [19]. PTEs were recently divided into two subclasses depending on the existence of an additional upstream hairpin that engages in a kissing-loop interaction (KL) with the 3' SL, an interaction that is required for efficient formation of the PK [17]. Many PTEs (and BTEs) contain the motif 5' UGCCA or its complement in the apical loop of their 5' SL, which participates in the long-distance RNA:RNA interaction with a 5' proximal hairpin apical loop or other unpaired sequence [20]. The PTE of pea enation mosaic virus 2 (PEMV2; umbravirus) is an exception by having a hairpin within an upstream 3'CITE (the adjacent "kissing loop T-shaped structure" [Kl-TSS]) engage in the long-distance interaction with the apical loop of a 5' proximal, coding region hairpin. The 3'TSS, found near the 3' end of several carmoviruses and umbraviruses, forms a tRNA-like structure [18] that directly interacts with ribosomes and 60S ribosomal subunits [21-23]. The connection between the 3'TSS and the 5' end remains uncertain, but has been proposed to involve bringing together 5'UTRbound 40S subunits with 60S-bound 3'TSS [22,23].

3'CITEs in members of the *Tombusviridae* are usually found near the 3' end of the gRNA and thus likely contain elements with secondary functions in initiation of minus-

strand synthesis [24,25]. For example, tobacco necrosis virus D (TNV-D) and red clover necrotic mosaic virus RNA1 contain novel purine-rich sequences just upstream of their BTE 3'CITE, which are important for both virus accumulation and translation [26,27]. In TCV, the 3'TSS 3'CITE is proposed to transit between alternative conformations when the genome is engaged in translation or replication, as binding of the RNA-dependent RNA polymerase (RdRp) to a location near the 3'TSS promoted a conformational shift that inhibited 3'TSS formation, causing a decrease in viral translation [24]. The TCV 3'TSS also serves as a scaffold for different interactions with surrounding elements, depending upon whether the region is bound by ribosomes or the RdRp [25,28].

Umbraviruses are unique within the *Tombusviridae* in having unusually long 3'UTRs (600 to 700 nt) containing several noncontiguous 3'CITEs in both the central region and proximal to the 3' end [29]. Umbraviruses have a single, (+)gRNA with four ORFs (Figure 1A); ORFs 1 and 2 are translated from the gRNA, and ORFs 3 and 4 are translated from a sgRNA. ORF 1 codes for a replication-related protein and ORF 2 encodes the RdRp, which is generated by a -1 ribosome frameshifting event near the end of ORF1. ORF 3 codes for an unstructured long-distance movement protein that also protects the sgRNA (and many cellular mRNAs) from nonsense-mediated decay [30]. ORF 4, which nearly completely overlaps with ORF 3, codes for a cell-to-cell movement protein in the 30K class of movement-related proteins [31]. For at least some umbraviruses, a second sgRNA is generated from the gRNA by a 5' to 3' exonuclease, which in opium poppy mosaic virus (OPMV) codes for an extension product of ORF 4 [8]. Umbraviruses do not encode a capsid protein or silencing suppressor and while they can independently infect some hosts, they depend upon a helper virus for vector transmission [30,32,33].

Umbravirus PEMV2 has three 3'CITEs; in the central portion of the 3'UTR is a PTE and upstream adjacent Kl-TSS, and a 3'TSS is proximal to the 3' end [9,34]. Using reporter constructs, the PEMV2 sgRNA was determined to require all three 3'CITEs for efficient translation in vivo, while gRNA constructs only required the Kl-TSS and PTE [21]. In contrast, OPMV contains two 3'CITEs, a centrally located BTE and the 3' proximal TSS [8], with only the BTE used by both gRNA and sgRNA2 reporter constructs for translation in vivo [8].

The presence of the PEMV2 PTE/Kl-TSS and the OPMV BTE in similar internal locations within their 3'UTRs led us to examine if other umbraviruses have known CITEs or "CITE-like" structures in the same location. Here, we report that such structures were not only evident, but nearly all umbraviruses contain their known or putative 3'CITE atop stem scaffolds just downstream from a very similar small hairpin with an internal loop and conserved sequence at the base and in the apical loop. Virtually all mutations in this "CITE-associated structure" (CAS) in OPMV and PEMV2 significantly reduced virus accumulation in *Nicotiana benthamiana* and many affected translation of cognate gRNA and sgRNA reporter construct, supporting an important function for the element in translation. Mutations in CAS did not substantially affect the structure of the adjacent 3'CITE but PEMV2 mutations significantly altered an upstream element conserved in 11 of 14 umbraviruses including OPMV. These results identify the CAS as a new, centrally located 3'UTR structure just upstream of different 3'CITEs that is critical for accumulation of umbraviruses and has differing effects on translation, suggesting the possibility that these umbravirus structures have evolved different functionalities.

2. Materials and Methods

2.1. Constructs

Plasmids pUC19-OPMV and pUC19-PEMV2 contain full-length OPMV and PEMV2 genomes, respectively, along with a T7 promoter upstream of the viral genome [8,35]. Similarly, in *Agrobacterium tumefaciens* binary vector pCB301, full-length OPMV and PEMV2 genomes were cloned downstream of the cauliflower mosaic virus 35S promoter,

and transformed into A. *tumefaciens*. Luciferase reporter constructs for OPMV gRNA (5'38+U) and sgRNA2 (5'69+U), and PEMV2 gRNA (5'89+U) and sgRNA and (5'128+U) were previously described [8,35]. Mutations in OPMV and PEMV2 constructs were introduced by QuikChange one-step site-directed mutagenesis [36] and were confirmed by sequencing (Eurofins Genomics).

2.2. In vitro transcription of full-length viral genomes

Restriction enzymes, SmaI and PvuII (New England BioLabs) were used to linearize pUC19-OPMV and pUC19-PEMV2, respectively, and OPMV and PEMV2 luciferase reporter constructs were linearized with SspI, followed by in vitro transcription using T7 RNA polymerase. In vitro transcribed RNAs were purified by lithium chloride precipitation. Transcripts were quantified using a DeNovix DS-11 FX spectrophotometer and quality was assessed by ethidium bromide-stained agarose gel electrophoresis.

2.3. RNA folding and SHAPE modification of RNA

As previously described [17], RNA transcripts (12 pmol) were denatured at 65 °C for 3 min and then cooled on ice for 2 min. RNA was incubated in folding buffer [80 mM Tris–HCl (pH 8.0), 11 mM Mg(CH $_3$ COO) $_2$, and 160 mM NH $_4$ Cl] for 10 min at 37 °C, and then divided into two equal portions. A final concentration of 15 mM of N-methylisatoic anhydride (NMIA) dissolved in dimethyl sulfoxide (DMSO) was added to the (+) folded RNA, while an equal volume of DMSO was added to the folded (–) negative modification control. (+) and (–) RNAs were incubated for 30 min at 37° C, ethanol precipitated and then resuspended in 11 μ l ddH $_2$ 0 for reverse transcription.

2.4. Reverse transcription of modified RNA

Primers used for SHAPE probing were: OPMV_R1: 5'-GGATGGGAGTGACCAC-CAC (positions 4235 – 4217), OPMV_R2: 5'-CAGAACCCTCAGTTTGACTAC (positions 4008 – 3988), PEMV2_R1: 5'-AGGAAACAGCTATGACC (positions 4319 to 4302), PEMV2_R2: 5'-CGCGTTTGTGATCTTTTTGG (positions 3959 to 3940). For primer extension reactions, 2.5 µM of PET-labeled and 6-carboxyfluorescein (FAM)-labeled oligonucleotides were used with 6 pmoles of unmodified RNA (for sequencing reactions) or NMIA- and DMSO-treated RNA (sample reactions). SuperScript III reverse transcriptase (Invitrogen) was used for reverse transcription reactions as previously described [37,38]. To perform fragment analysis, cDNA products with ladders generated by Sanger sequencing were sent to Genewiz. Files related to fragment analyses were processed and analyzed using QuShape [39]. To verify that QuShape correctly subtracted the background from the corresponding peak positions, manual adjustments were implemented. RNA secondary structures were initially obtained using mFold [40] and modified by phylogenetic comparisons.

2.5. Agroinfiltration and RNA gel blot analysis

OPMV and PEMV2 binary vector constructs were transformed into A. *tumefaciens* strain GV3101 and cultured in the presence of antibiotics. Cells were harvested and resuspended in resuspension buffer (10 mM MgCl₂, pH 5.7, and 100 μ M acetosyringone). For infiltrations of OPMV/PEMV2 WT and mutant constructs, an OD₆₀₀ of 0.6 was mixed with the pothos latent virus p14 silencing suppressor construct [8] at an OD₆₀₀ of 0.2 and infiltrated into two fully expanded leaves of N. *benthamiana*. After 72 h, agroinfiltrated leaves were harvested, and TRIzol (Invitrogen) was used to isolate total RNA. For RNA gel blot analysis, RNA was subjected to electrophoresis through 2% agarose gels and transferred to a charged nylon membrane by capillary action in 4X SSC (1X SSC is 0.15 M NaCl plus

0.015~M sodium citrate) buffer. After UV cross-linking, membranes were hybridized with a mixture of three [α^{-32}] dATP-labeled DNA oligonucleotides complementary to OPMV positions 3591 to 3630, 3634 to 3672, and 3676 to 3715. For PEMV2, a mixture of three [α^{-32}] dATP-labeled DNA oligonucleotides complementary to positions 2731 to 2771, 2969 to 3004, and 3229 to 3270 were used. After incubation and washing, nylon membranes were exposed to a phosphorimager screen and scanned using an Amersham Typhoon Biomolecular Imager. Raw images were processed using ImageJ software to produce gel images and to quantify band intensities.

2.6. Protoplast transfection and in vivo luciferase assays

Protoplasts prepared from callus cultures of *Arabidopsis thaliana* were transfected with luciferase reporter transcripts using a polyethylene glycol-mediated transformation protocol as previously described [35]. Briefly, 5×10^6 protoplasts were transfected with 20 μ g of OPMV/PEMV2 luciferase reporter transcripts and incubated under constant light for 18 h at 22 °C. Cells were lysed at 18 h post-transfection, and luciferase activity was assayed with a dual-luciferase reporter assay system (Promega) using a Modulus microplate multimode reader (Turner BioSystems).

2.7. RNA structure drawing

All RNA structures were generated using the on-line RNA2Drawer web app (https://rna2drawer.app) [41].

3. Results

3.1. All umbraviruses contain a conserved hairpin in their 3'UTR located upstream of known or putative 3'CITEs

Sequences upstream of internally located, previously defined 3'CITEs were aligned to identify any nearby conserved elements that might also play a role in translation. Just upstream (7 to 15 nt) from the base of a putative scaffold supporting known BTE 3'CITEs was a region with three discontinuous conserved motifs capable of folding into a small hairpin with an internal loop (Figures 1B top, 2). All hairpins contained one of the conserved motifs fully or partially in the apical loop, with the other conserved sequences located at the base of the stem extending into flanking sequences on both sides. Analysis of the same region in non-BTE containing umbraviruses revealed that the same conserved sequences were present (Figure 1B, bottom), which for PEMV2 were similarly located just upstream from a putative scaffold containing its PTE and Kl-TSS 3'CITEs (Figure 3). The four umbraviruses without known 3'CITEs (PasUV1, CMoMV, RCUV, and CMoV) were predicted to have "CITE-like" structures atop scaffolds in identical locations downstream from the conserved hairpin (Figures 1B bottom, and 3). This positionally and partial sequence-conserved hairpin has been designated as the CITE-associated structure or CAS.

In addition, a second structurally conserved element was found 0 or 1 nt upstream of CAS in all BTE-containing umbraviruses and two non-BTE umbraviruses (PEMV2 and RCUV). This element consists of two similar-sized stem-loops (SLX and SLY) separated by 6 to 11 nt. SLX and SLY apical loops contain 3 to 6 residues capable of canonical basepairing, thus forming a KL between the two stem-loops (Figures 1C, 2 and 3). For three umbraviruses, the KL included the motifs "GCCA" and "UGGC", previously identified as common tertiary interacting motifs in umbraviruses and carmoviruses [20,35]. SLX, SLY and the putative KL are referred to as the "KL element" in this report.

3.2. SHAPE RNA structure probing of OPMV gRNA and sgRNA CAS region

To investigate if the predicted structures of the CAS and KL element are present in

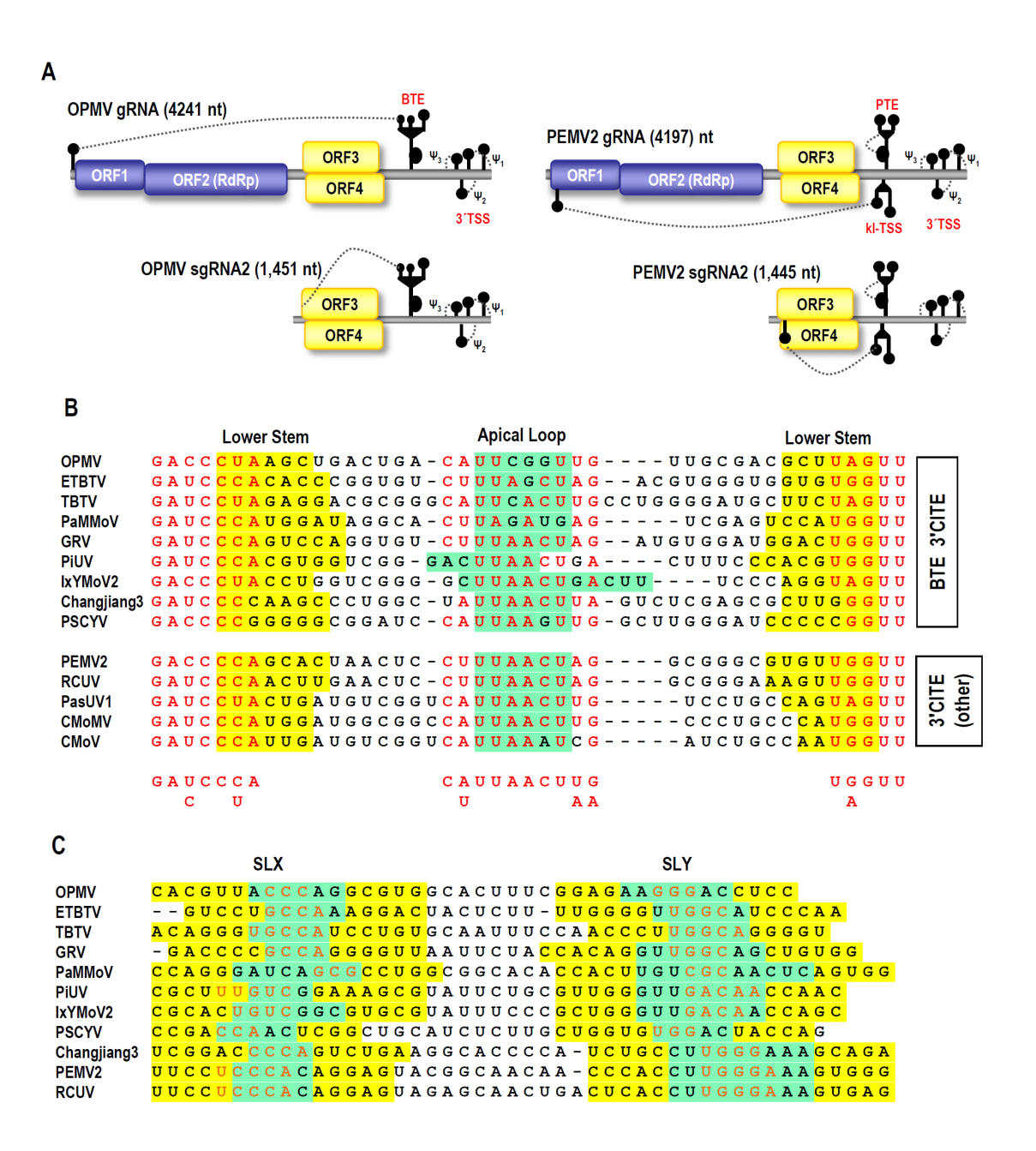


Figure 1. Novel conserved structures in the 3'UTR of umbraviruses. A. Umbravirus genome organization. Replication-required proteins are in blue and movement proteins are in yellow. A second, slightly larger sgRNA is present in some umbraviruses including OPMV. 3'CITEs are shown along with the long-distance interaction (dashed line) connecting some 3'CITEs to the 5' end. B. Sequence alignment in CAS region. Conserved residues are in red. Residues in the CAS apical loop are shaded green and residues in the lower stem are shaded yellow. C. Conserved structures just upstream of CAS in 11 umbraviruses. Two hairpins (SLX and SLY) are denoted with stem sequences in yellow and apical loops in green. Putative kissing loop sequences are in orange. OPMV, opium poppy mosaic virus; ETBTV, Ethiopian tobacco bushy top virus; TBTV, tobacco bushy top virus; PaMMoV, patrinia mild mottle virus; GRV, groundnut rosette virus; PiUV, picris umbravirus 1; IxYMoV2, ixeridium yellow mottle virus; Changjiang3, Changjiang tombus-like virus 3; PSCYV, paederia scandens chlorosis yellow virus; PEMV2, pea enation mosaic virus 2; RCUV, red clover umbravirus; PasUV1, Paederia scandens chlorosis yellow umbravirus; CMoW; carrot mottle mimic virus; CMoV, carrot mottle virus.

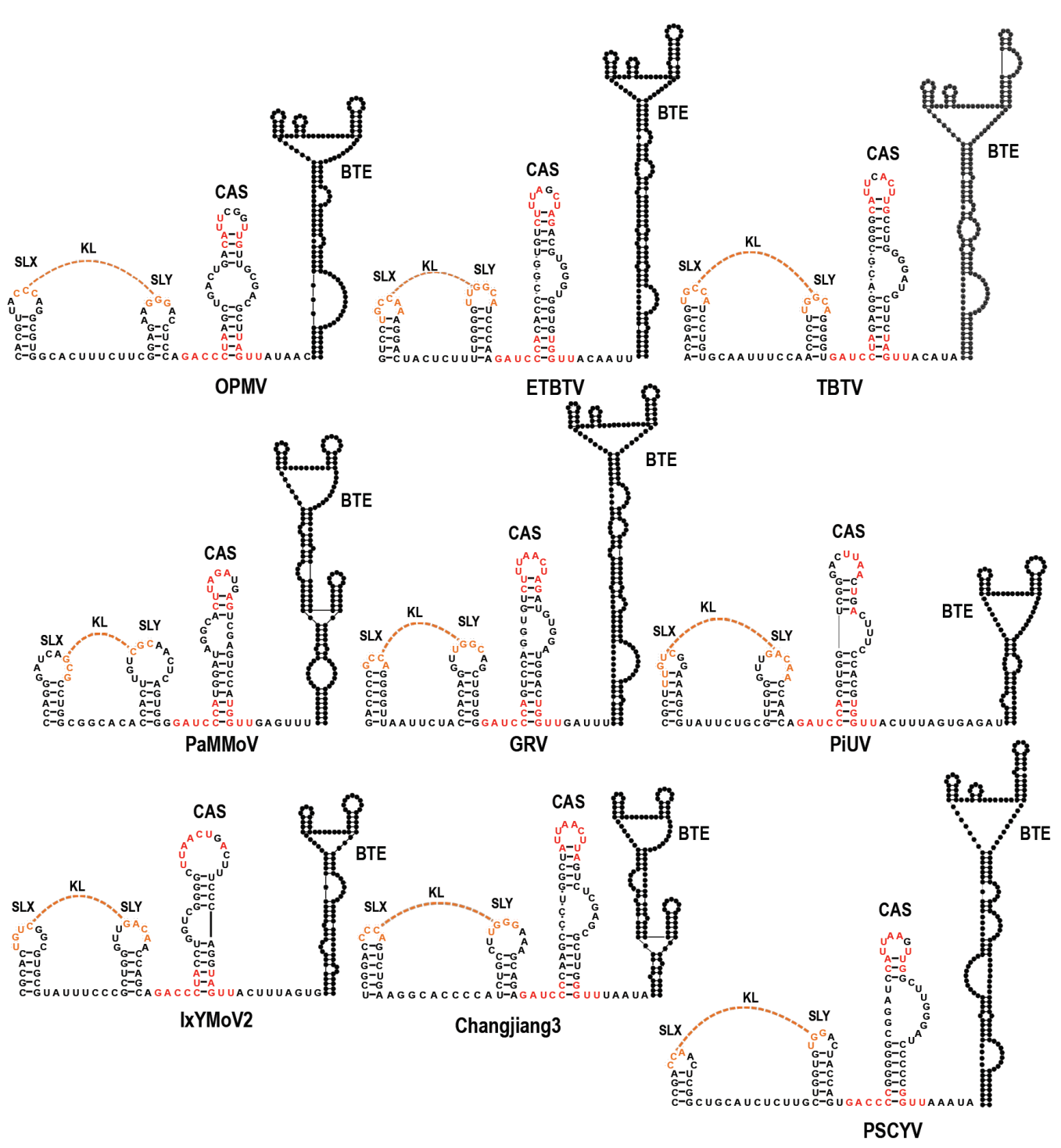


Figure 2. Predicted structures in the central region of umbraviruses containing BTE 3'CITEs. Conserved CAS sequences are in red. KL sequences are in orange. Each dot of the BTE represents a nucleotide.

OPMV transcripts, full-length gRNA and sgRNA2 transcripts were synthesized in vitro, denatured by heat and renatured by cooling, and then subjected to Selective 2' Hydroxyl Acylation analyzed by Primer Extension (SHAPE) RNA structure probing (Figure 4). SHAPE reports on the flexibility of residues, with unpaired residues usually being more flexible and thus more capable of assuming a conformation necessary for interaction with SHAPE reagents. SHAPE reactivities for both OPMV gRNA and sgRNA2 residues were similar in the CAS and BTE region and consistent with the presence of SLX, SLY and the

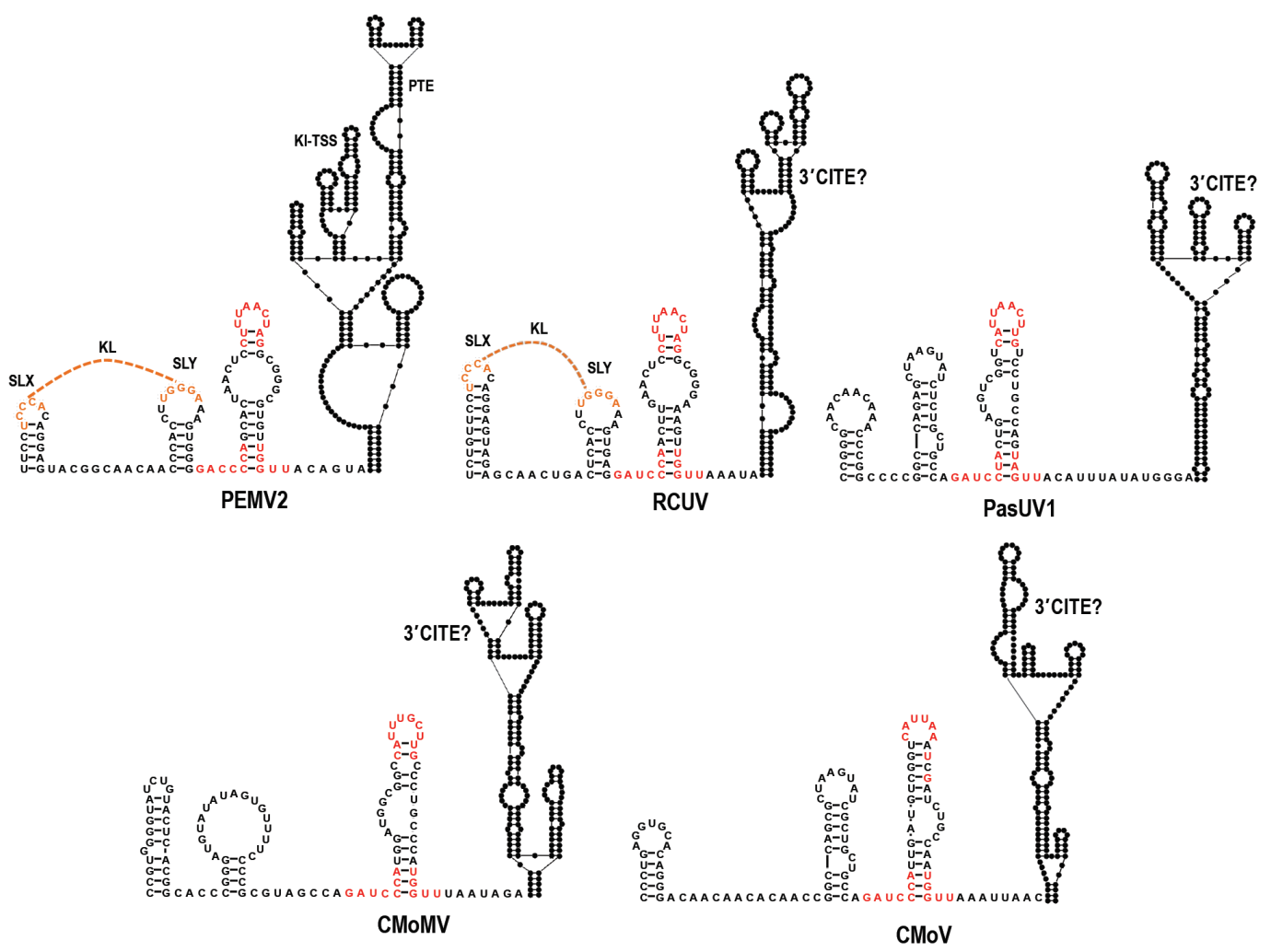


Figure 3. Predicted structures in the central region of umbraviruses containing non-BTE 3'CITEs. Conserved CAS sequences are in red. KL sequences are in orange. Putative 3'CITEs are denoted by a question mark.

KL. However, the lower CAS stems in both gRNA and sgRNA2 transcripts were not supported by SHAPE data, as both contained similar SHAPE-reactive residues on the 5' side (Figure 4). In contrast, the BTE structures for both gRNA and sgRNA were well supported by SHAPE data, as was previously shown for the gRNA [8], with similar SHAPE-reactive residues mainly in unpaired regions. One prominent exception was the base of the BTE scaffold, with three residues on the 5' side and 2 on the 3' side being reactive with the SHAPE reagent.

3.3. OPMV CAS is important for viral accumulation in vivo

To test for the importance of the phylogenetically conserved OPMV CAS structure, deletions and base modifications were introduced into base-paired and apical and internal bulge loop CAS sequences (Figure 5A). WT and mutant gRNA accumulation was assessed by RNA gel blots following *Agrobacterium tumefaciens*-mediated infiltration of expression constructs into N. *benthamiana*. Conversion of the conserved CAS 6 nt apical loop into a UNCG-type tetraloop (mC1) decreased virus accumulation by 7-fold (Figure 5B). Deletion of the upper portion of CAS, including the internal bulge (mC2), or alteration of three

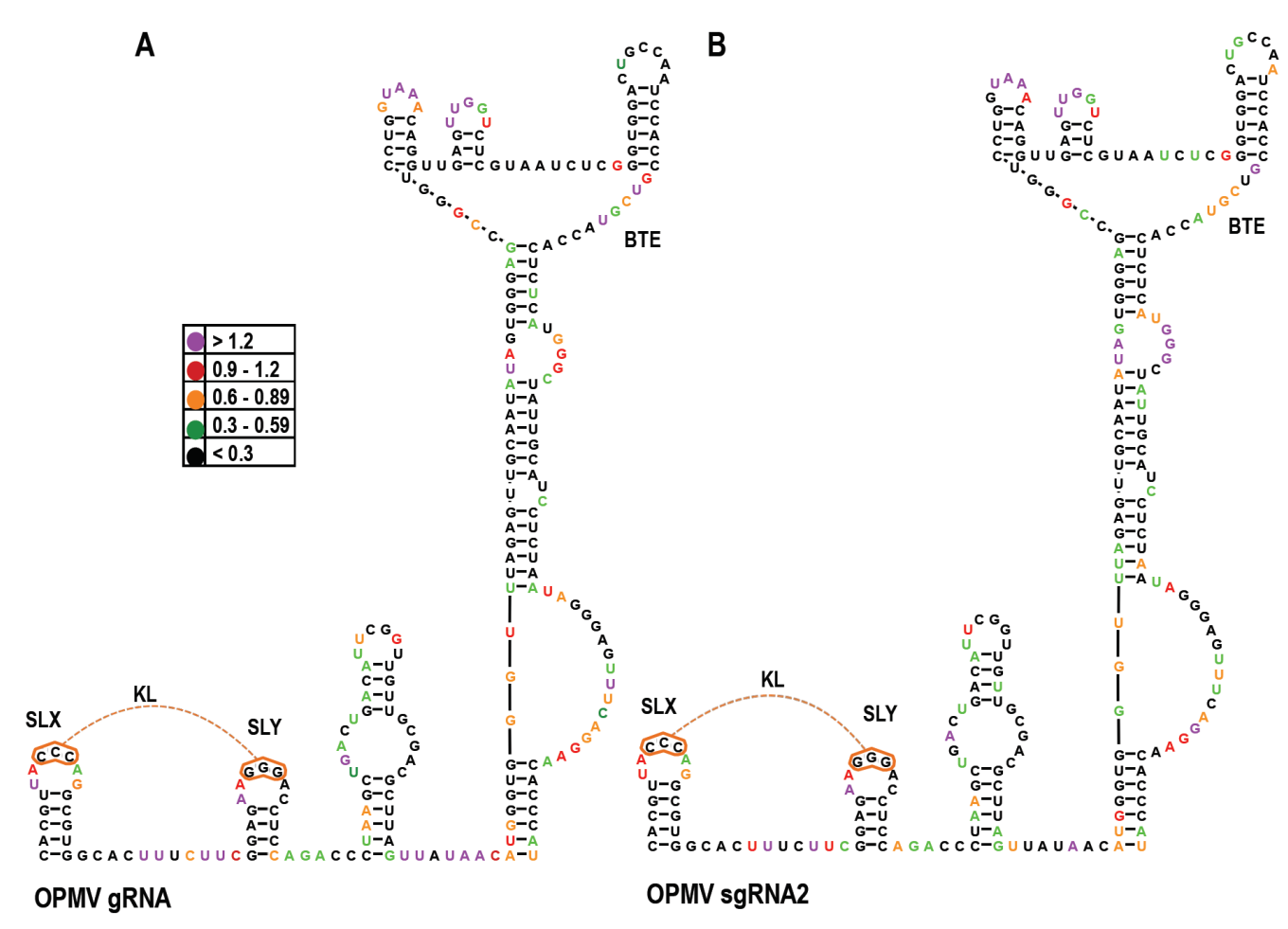


Figure 4. SHAPE RNA structure probing of the OPMV CAS region in full-length gRNA and sgRNA2 transcripts. A. SHAPE was conducted using fluorescently-labeled primers, which differed experimentally from previous SHAPE probing of gRNA OPMV 3'UTR (8) but generated similar results. Individual residue "dots" are colored according to NMIA reactivity, from purple (most reactive) to black (least reactive). gRNA structures are labeled for clarity. B. SHAPE data for the CAS region in full-length OPMV sgRNA2 transcripts.

residues on the 3' side of the bulge (mC3) reduced virus accumulation to near undetectable levels. Surprisingly, deletion of the entire CAS (mC4) was not as detrimental, with the gRNA reaching 11% of WT levels. To address the presence of the CAS hairpin structure, single and compensatory mutations were introduced into the lower stem. Single mutations mC5 and mC6 were both detrimental, reducing virus accumulation to 17 and 50% of WT levels, respectively. mC5+mC6, which should reestablish the lower stem, restored virus accumulation to greater than WT levels. Altogether, these results strongly support the phylogenetically conserved CAS structure and the importance of the element for efficient accumulation of OPMV in N. benthamiana.

3.4. OPMV CAS is required for efficient translation of gRNA and sgRNA2 reporter constructs in vivo

The conserved location of CAS hairpins just upstream of known or putative 3'CITEs in all umbraviruses suggested a possible conserved function in translation mediated by the adjacent 3'CITE. To begin testing this hypothesis, CAS deletions and base alterations

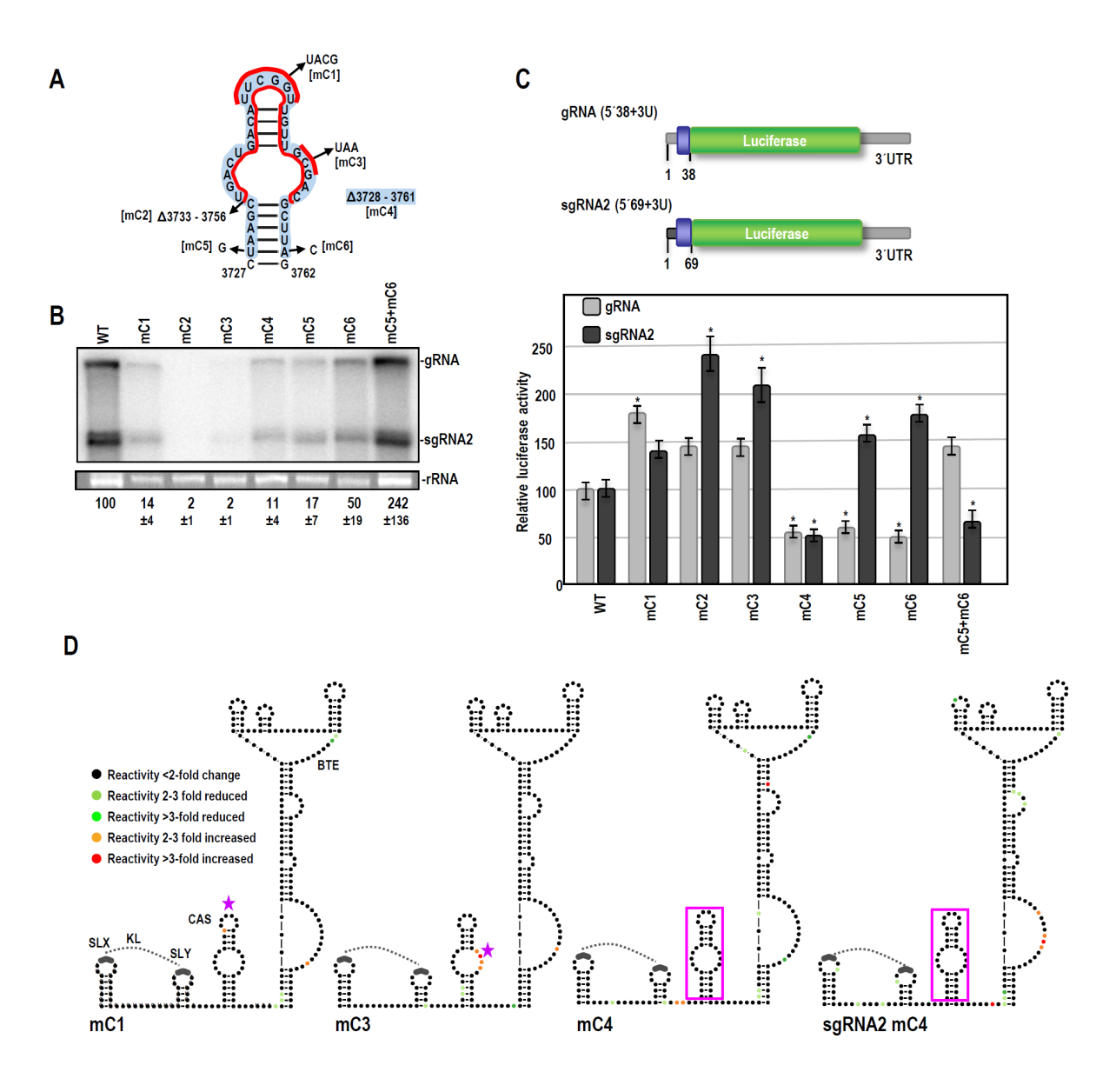


Figure 5. CAS is important for OPMV accumulation in N. benthamiana and efficient translation of reporter constructs. A. CAS nucleotide alterations and deletions. Names of mutations are in brackets. Red lines help define some of the mutations and deletions. B. RNA gel blot analysis of total RNA extracted from systemically infected N. benthamiana following agroinfiltration with either WT or mutant OPMV. Ethidium bromide-stained 26S rRNA was used as the loading control. Standard error is shown for three independent experiments. C. Relative translation of OPMV gRNA and sgRNA reporter transcripts containing full-length 3'UTR, and 5' terminal sequences [non-coding (gray) and coding (blue)] necessary for efficient translation as previously described (8). gRNA construct; 5' terminal 38 nt (5'38+U). sgRNA2 construct; 5' terminal 69 nt (5'69+U). Luciferase activity was assayed 18 h following protoplast transfection. Error bars denote standard deviation for three independent assays. '*' Denotes statistical difference with P < 0.05. D. SHAPE RNA structure probing of selected OPMV gRNA and sgRNA full-length CAS mutant transcripts. Colors denote changes in mutant nucleotide reactivity relative to WT. Black dots, < 2-fold change; light green, 2- to 3-fold reduction; dark green; > 3-fold reduction; orange, 2- to 3-fold increase; red, >3-fold increase. Pink star denotes location of alteration. CAS deletion is boxed in magenta. SHAPE data averaged from at least 3 independent replicates.

were introduced into firefly luciferase reporter constructs previously used to analyze sequences involved in translation of the gRNA and sgRNA2 (Figure 5C). Both constructs contain the full-length 3'UTR along with 5' sequences sufficient for efficient translation, which includes the BTE long-distance interacting motif. This required that the gRNA construct include the gRNA 5' terminal 38 nt (5'38+U) and the sgRNA2 construct include the sgRNA 5' terminal 69 nt (5'69+U). Transcripts were transformed into A. thaliana protoplasts, and luciferase activity was measured 18-hours later. CAS apical loop mutation mC1 increased 5'38+U luciferase activity by 1.8-fold but did not significantly affect translation of 5'69+U (Figure 5C). Removal of the top half of the CAS (mC2) or mutations in the bulge (mC3) enhanced translation of 5'38+U by nearly 50% (although this increase was not considered significant). Translation of 5'69+U increased by 2.1- and 2.4-fold, respectively, suggesting that the upper portion of CAS contains a translation repressor. In contrast, complete removal of CAS (mC4) caused a 2-fold decrease in translation of both 5'38+U and 5'69+U. Disruption of the lower CAS stem (mC5 and mC6) had contrasting effects for the gRNA and sgRNA constructs, decreasing luciferase activity by ~2-fold in 5'38+U while increasing luciferase activity by 1.6- and 1.8- fold in 5'69+U. Reestablishing the lower stem (mC5+mC6) reversed the effects of the single mutations, increasing translation of 5'38+U to a level greater than WT and decreasing translation of 5'69+U. These results support an important but differential role for CAS in translation of the gRNA and sgRNA constructs associated with specific 5'-proximal sequences, the only difference between the two constructs.

3.5. Effect of OPMV CAS mutations on BTE and KL structures

To address how CAS might be impacting translation, and assess its direct or indirect connection (if any) with the upstream KL element and downstream BTE, full-length OPMV gRNA transcripts containing a subset of the CAS mutations were subjected to SHAPE structure probing (Figure 5D). Data is color coded for individual residues, with orange and red representing SHAPE reactivity increases of 2- fold or >2-fold, respectively, and light green and dark green representing reactivity decreases of 2- fold or >2-fold, respectively.

Altering the CAS apical loop (mC1) did not significantly change residue reactivity in the KL element (i.e., less than a 2-fold change), suggesting that the KL element is not interacting with the conserved CAS apical loop. In contrast, residues on the 5' side of the BTE scaffold lower stem that were normally reactive by SHAPE (see Figure 4A) had significantly reduced reactivity, as did two residues in the upper portion of the BTE that are part of a conserved BTE motif [8]. The remainder of the BTE was virtually unchanged, suggesting that the conserved apical loop was likely not directly interacting with the 3'CITE.

CAS interior bulge mutation (mC3) caused a substantial increase in reactivity of residues at the mutation site, suggesting that this bulge sequence is paired in the WT gRNA transcript (Figure 5D). Additionally, residues that were normally SHAPE reactive in the CAS lower stem showed a significant reduction in reactivity, suggesting that CAS was now assuming its phylogenetically conserved hairpin structure. The single reactive residue in the stem of SLY in WT transcripts was also significantly less reactive, suggesting stabilization of the SLY stem-loop. Only a single BTE residue (in the large bulge loop near the base) showed enhanced reactivity, suggesting that the WT bulge loop sequence was not interacting with the BTE.

Deletion of the entire CAS hairpin (mC4) caused similar reductions in reactivity in the BTE lower stem and upper conserved motif as mC1, likely a consequence of removing the conserved CAS apical loop sequence (Figure 5D). Four additional scattered residues in the BTE displayed reactivity changes due to the CAS deletion. The single residue in SLY that showed reactivity reduction for mC3 was similarly reduced in mC4 transcripts, suggesting a similar consequence associated with loss of these CAS bulge loop sequences.

When sgRNA2 transcripts with the CAS deletion (mC4) were subjected to SHAPE structure probing, both similar and unique changes in residue reactivity were evident. In the BTE, very similar reactivity reductions were found at the base of the BTE and in the upper conserved motif, suggesting that loss of the CAS apical loop sequences in the sgRNA had similar BTE structural consequences. Two additional bulge loop regions in the BTE were uniquely altered: the upper bulge (and closing base-pair) had 3 of 7 residues with reduced reactivity while the large bulge near the BTE base had 4 residues with enhanced reactivity. In the KL element, one residue in the loops of the SLX and SLY hairpins had reduced reactivity along with two residues between the two hairpins. Since gRNA and sgRNA2 share identical sequences in this location, these results suggest that this location does not constitute a structurally separate domain in gRNA and sgRNA2 transcripts, but is interacting with sequences in the gRNA that are missing in the sgRNA2 or that assume a different conformation.

3.6. Examination of conserved CAS flanking sequence and a complementary sequence in the BTE 17-nt signature motif

As shown in Figures 1B, 2 and 3, sequence flanking both sides of the CAS are strongly conserved in all umbraviruses. Curiously, the upstream flanking sequence, 5'GA C/U CC, is complementary to sequence at the 5' end of the 17-nt conserved motif in 7 of 9 umbravirus BTEs (5'GG G/A UCCUGGUAAACAGG), including a covariant change in OPMV when compared with other umbraviruses (Figure 6A). To determine if there is a direct interaction between the CAS and BTE mediated by these sequences, single mutations were individually generated in the two motifs, converting them into the same sequence found majority of BTE-containing umbraviruses (5'GACCC:GGGUC 5'GA<u>U</u>CC:GG<u>A</u>UC). The BTE mutation G3808A, which should disrupt the putative interaction while maintaining a consensus 17-nt BTE signature sequence, reduced OPMV accumulation in N. benthamiana to near undetectable levels (Figure 6B). In contrast, the corresponding mutation upstream of the CAS (C3726U), which maintains the conserved consensus sequence while disrupting the putative CAS-BTE interaction, had no effect on OPMV accumulation in N. benthamiana. When present together in the same transcript, OPMV levels were enhanced nearly 6-fold compared with G3808A alone, suggesting a possible slight compensatory effect. However, the mutant OPMV still accumulated poorly (23% of WT) despite containing the more conserved versions of the two motifs.

Since mutagenesis assays did not conclusively rule in (or out) an interaction between the two conserved motifs, transcripts containing the single and double mutations were subjected to SHAPE structure probing. Our reasoning was that disruption of an interaction between the two motifs should cause structural changes in the partner sequence that might be reduced by the compensatory mutations. C3726U caused enhanced reactivity at the mutation site upstream of CAS, suggesting that this sequence is normally paired (Figure 6C). However, no reactivity changes were evident in the proposed interacting BTE motif although several BTE residues showed reduced reactivity. BTE mutation G3808A both enhanced and reduced reactivity of residues at the mutation site and at several other sites in the BTE, but not in the corresponding motif upstream of CAS. Transcripts containing both C3762U and G3808A showed an additive effect of the changes due to the individual mutations, as well as a substantial number of additional reactivity changes in the BTE and other sequences in the region (Figure 6C). Therefore, SHAPE data do not support a direct interaction between the two conserved motifs in the initial structure assumed by these transcripts.

3.7. Disrupting the KL between SLX and SLY does not affect accumulation in N. benthamiana

Eleven of 14 umbraviruses have a similarly positioned KL element (Figure 1C, 2 and 3). To test for the presence and importance of the KL interaction in accumulation of OPMV in N. *benthamiana*, single and compensatory mutations were generated and levels were

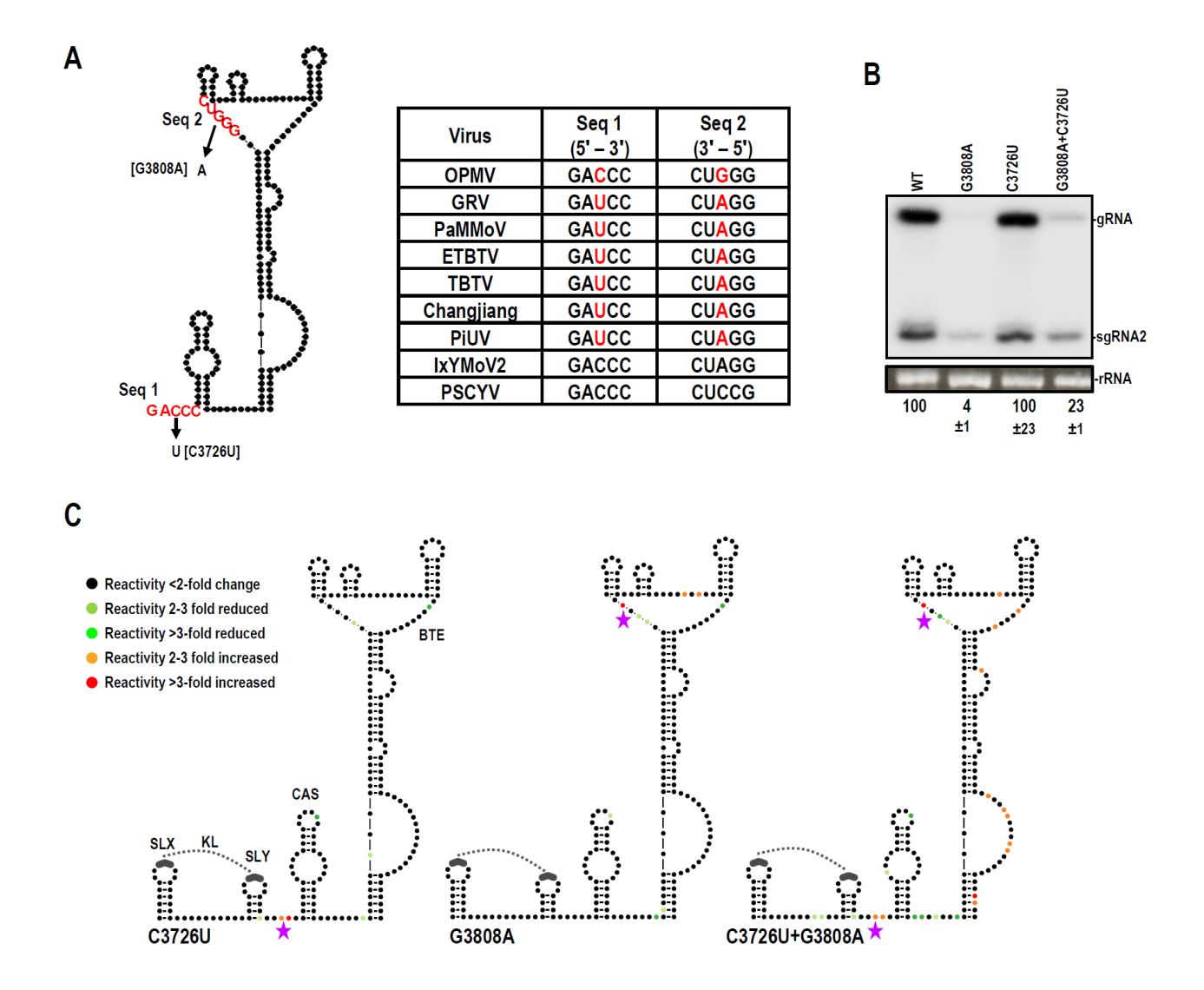


Figure 6. Direct interaction between CAS- and BTE-conserved sequences is not supported by SHAPE. A. Location of the alterations and Table showing conserved sequence just upstream of CAS that can potentially pair with conserved sequence in the BTE. OPMV contains a covariant change not present in other umbraviruses. B. RNA gel blot analysis of total RNA extracted from systemically infected N. *benthamiana* following agroinfiltration with either WT OPMV or CAS/BTE mutants. Ethidium bromide-stained 26S rRNA was used as a loading control. Standard error is shown from three independent experiments. C. SHAPE probing of OPMV gRNA mutants. Colors represent changes in nucleotides reactivity relative to WT. See legend to Figure 5. Star indicates location of alterations. SHAPE data was averaged from at least 3 independent replicates.

determined by RNA gel blots (Figure 7). gRNAs containing single and double mutations accumulated between 81 and 84% of WT OPMV, a decrease that was not significant. The purpose of this putative KL interaction conserved in the majority of umbraviruses thus remains unknown.

3.8. SHAPE RNA structure probing of the PEMV2 gRNA and sgRNA3'UTR

To examine if CAS alternations in other umbraviruses lead to similar effects on virus accumulation, translation, and structural alterations in the 3'CITE region, the CAS of

PEMV2 with its upstream KL element and downstream PTE/Kl-TSS 3'CITEs was also investigated. Figure 8A shows that full-length gRNA and sgRNA transcripts have similar SHAPE structure profiles in this region. However, unlike SHAPE data for the OPMV CAS, PEMV2 SHAPE data was consistent with the presence of the CAS structure in both gRNA and sgRNA transcripts (Figure 9B). Also, unlike OPMV, SLX was not supported in the gRNA transcripts and neither SLX nor SLY were supported in the sgRNA transcripts. These data suggest that different umbraviruses may assume different conformations in this region.

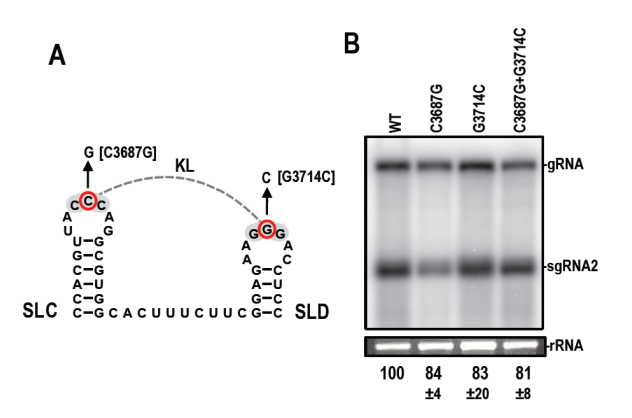


Figure 7. Disruption of the putative KL between SLX and SLY does not affect accumulation of OPMV in infiltrated leaves. A. C3687G and G3714C (indicated by red circles) were introduced to disrupt a KL. B. RNA gel blot analysis of total RNA extracted from systemically infected *N. benthamiana* following agroinfiltration with either WT OPMV, or OPMV containing either single or double mutations. Ethidium bromide-stained 26S rRNA was used as a loading control.

3.9. CAS is required for efficient accumulation of PEMV2 in vivo

Mutations similar to those used to investigate the OPMV CAS were introduced into PEMV2 CAS and effect on viral accumulation was similarly assessed by RNA gel blot analysis following A. *tumefaciens*-mediated infiltration of expression constructs in N. *benthamiana* (Figure 9A). Similar to OPMV CAS, converting the apical loop sequence into a UNCG tetraloop (PCm1), deletion of the upper portion of CAS (PCm2), alteration of residues in the internal loop (PCm3), or complete CAS deletion (PCm4) all reduced PEMV2 accumulation below the level of detection (Figure 9B). Single residue changes near the base of the stem (PCm5 and PCm6) reduced accumulation to 68% and below the level of detection, respectively, and similar to OPMV, the compensatory mutations together enhanced accumulation to greater than WT levels. These results confirm an important function for CAS in umbraviruses with different 3'CITEs.

3.10. PEMV2 CAS is required for efficient translation of gRNA but not sgRNA reporter constructs in vivo

The same mutations used to study effects of OPMV CAS on translation were introduced into PEMV2 gRNA and sgRNA luciferase constructs (Figure 9C). Both constructs contained the complete 703 nt PEMV2 3'UTR, with the gRNA construct containing the 5' 89 nt of the gRNA (5'89+U) and the sgRNA construct containing the 5' 128 nt of the sgRNA (5'128+U) to accommodate the KI-TSS long-distance RNA:RNA interacting sequences. Similar to OPMV, PmC1 increased luciferase activity of the gRNA construct by 1.7-fold relative to WT and did not significantly affect sgRNA luciferase activity, suggesting a possible related function for the conserved CAS apical loop as a translation repressor in the gRNA (Figure 9C). In contrast with OPMV, PmC2 and PmC3 did not significantly

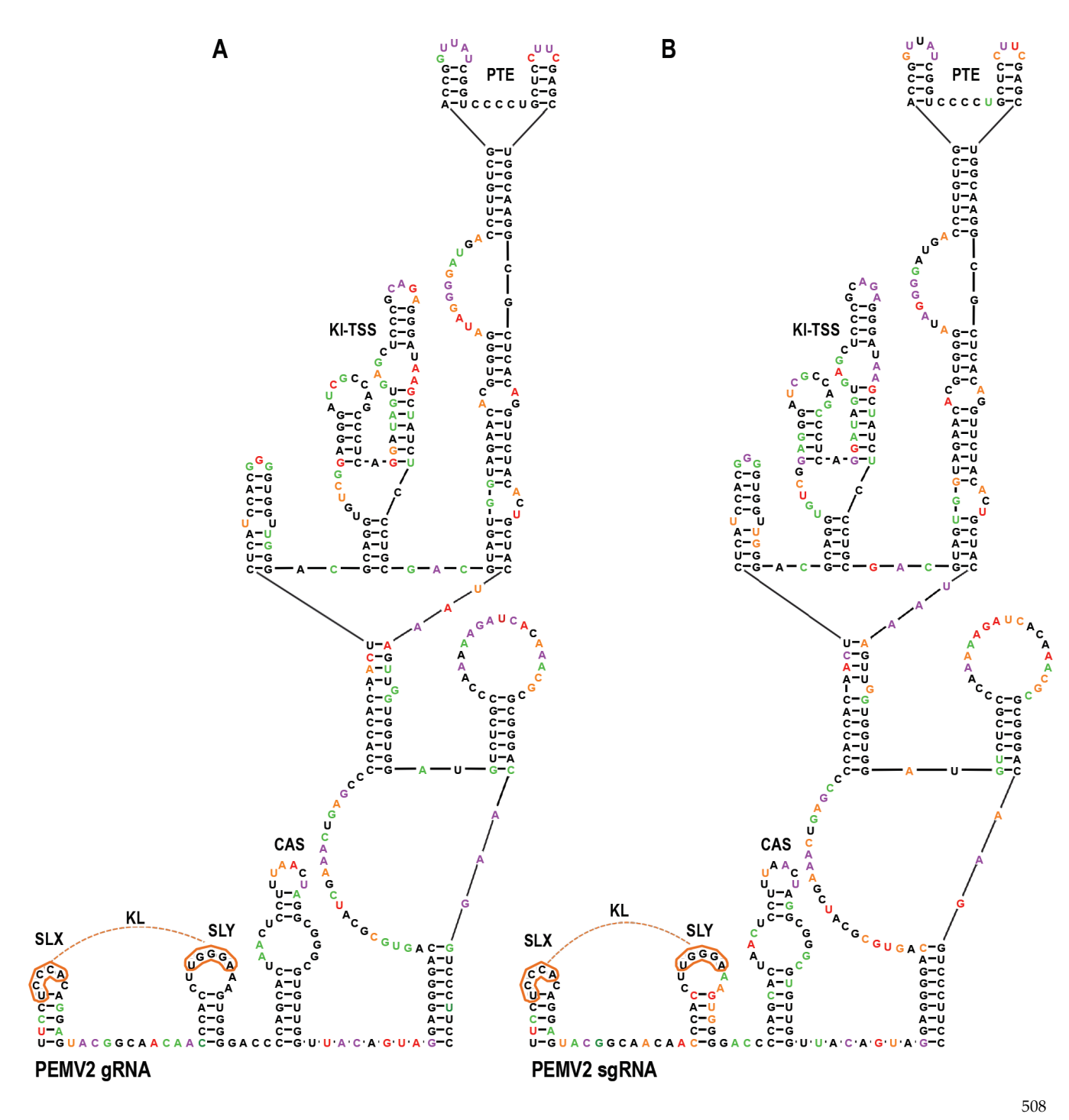


Figure 8. SHAPE probing of the CAS region in full-length PEMV2 gRNA and sgRNA. A. SHAPE reactivity of gRNA residues. Dots are colored according to SHAPE NMIA reactivity. See legend to Figure 4. B. SHAPE reactivity of sgRNA residues.

affect translation of either the gRNA or sgRNA reporter constructs. Deletion of CAS (PmC4) decreased gRNA luciferase activity 5-fold relative to WT, but unlike OPMV did not similarly affect translation of the sgRNA construct. PmC5, PmC6, and PmC5+PmC6 had little effect on translation of the PEMV2 gRNA and sgRNA constructs, unlike the differential effects of the analogous OPMV mutations. These results suggest that, with the exception of the apical loop, PEMV2 CAS is functioning differently from OPMV CAS in supporting and repressing translation of gRNA and sgRNA constructs.

523

524

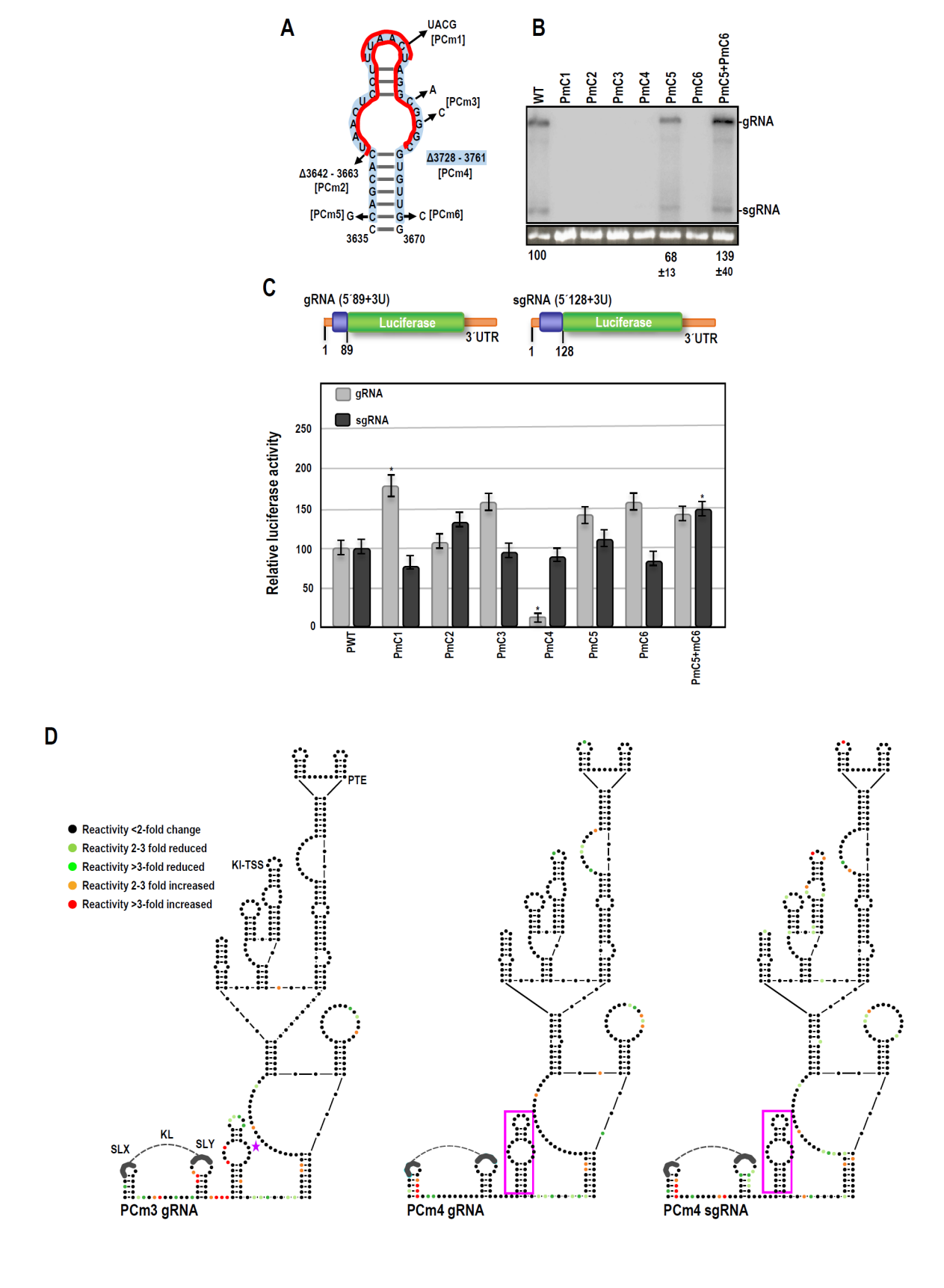


Figure 9. PEMV2 CAS is important for virus accumulation and efficient translation of gRNA reporter construct. A. Locations of mutations in the CAS hairpin. Names of mutations are bracketed. Red lines indicate some of the nucleotides that were altered or

527

528

529

530

531

533

535 536

537

538

539

540

541

542

543

545

546

547

548

549

550

551

552

554

555

556

557

558

559

561

562

deleted. B. RNA gel blot analysis of total RNA extracted from systemically infected N. benthamiana leaves following agroinfiltration with either PEMV2 WT or derived CAS mutants. Ethidium bromide-stained 26S rRNA was used as a loading control. C. PEMV2 reporter constructs containing complete 3'UTR and 5' end non-coding (orange) and coding (blue) sequences as previously described (35). Relative luciferase activity of constructs was assayed in protoplasts. Error bars denote standard deviation for three independent assays. D. SHAPE RNA structure probing of PEMV2 gRNA and sgRNA CAS mutants. Dot colors represent changes in nucleotides reactivity in the mutant construct relative to WT (see legend to Figure 5). Star indicates position of the mutation.

3.11. PEMV2 CAS mutations affect the structure of upstream sequences

To determine the effects of CAS mutations on the structure of the PEMV2 3'CITEs and upstream KL element, full-length gRNA transcripts containing PCm3 and PCm4 were analyzed by SHAPE structure probing (Figure 9D). Unlike OPMV Cm3, PCm3 caused significant reactivity changes in CAS and surrounding regions, including: (1) enhanced reactivity in the SLX and SLY stems; (2) enhancement and reduction of residue reactivity between SLX and SLY; (3) substantially enhanced reactivity of the conserved "GAUC" adjacent to CAS; and (4) reactivity differences throughout CAS, including reduced reactivity of 5 of 7 residues in the apical loop; and (5) reduced reactivity of the sequence between CAS and the 3'CITE structure. Similar to OPMV CAS Cm3, only scattered differences were found within the downstream 3'CITE structure, including two consecutive residues in the base stem, and none within the KI-TSS and PTE 3'CITEs.

Deletion of CAS (PCm4) also caused a number of SHAPE reactivity changes both upstream and downstream of the deletion. Most prominent reactivity changes were enhanced reactivity in SLX stem residues, and similar to PCm3, reduced reactivity of residues between the CAS and the 3'CITE structure and enhanced reactivity of the same two residues in the base stem of the 3'CITE structure (Figure 9D). Deletion of CAS also caused reactivity changes in the bulge loop of the PTE, a critical region that forms a required pseudoknot within the CITE. Since deletion of CAS gave very different outcomes for translation of the gRNA and sgRNA reporter constructs, sgRNA PCm4 transcripts were also subjected to SHAPE probing. Whereas CAS deletion in the sgRNA caused similar changes in SLX and in the sequence between the CAS and the 3'CITE structure as found for the gRNA, a substantial number of differences were present likely due to the existence of additional sequence and/or different structures outside of this region between the gRNA and sgRNA transcripts. These results strongly suggest that PEMV2 CAS, unlike OPMV CAS, has a direct or indirect structural connection with the upstream KL element and sequences between the CAS and the 3'CITE structure. Overall, our results support CAS as a critical new translation element in umbraviruses, whose overall mode of action likely differs depending on the virus and whether the template is gRNA or sgRNA.

4. Discussion

Many plus-strand RNA plant viruses follow unconventional translational pathways often mediated by 3'CITEs present near the 3' end of viral genomes [24-26]. Umbraviruses are unusual in having extended 3' UTRs that contain multiple, 3'CITEs with different usages for translation of gRNA and sgRNA [21]. In this report, we identify an additional critical umbravirus element, the CAS, located just upstream of all centrally located 3'CITEs. All umbravirus CAS share conserved features including highly conserved residues in their apical loops and at the base of the stem extending into flanking sequences, along with an internal bulge loop that can be symmetrical or asymmetrical. The 3'CITEs just downstream of the CAS are predicted to be perched atop extended supporting stems (with the exception of PiUV), placing CAS a short distance upstream from the base

563 564 565

566

567

569 570 571

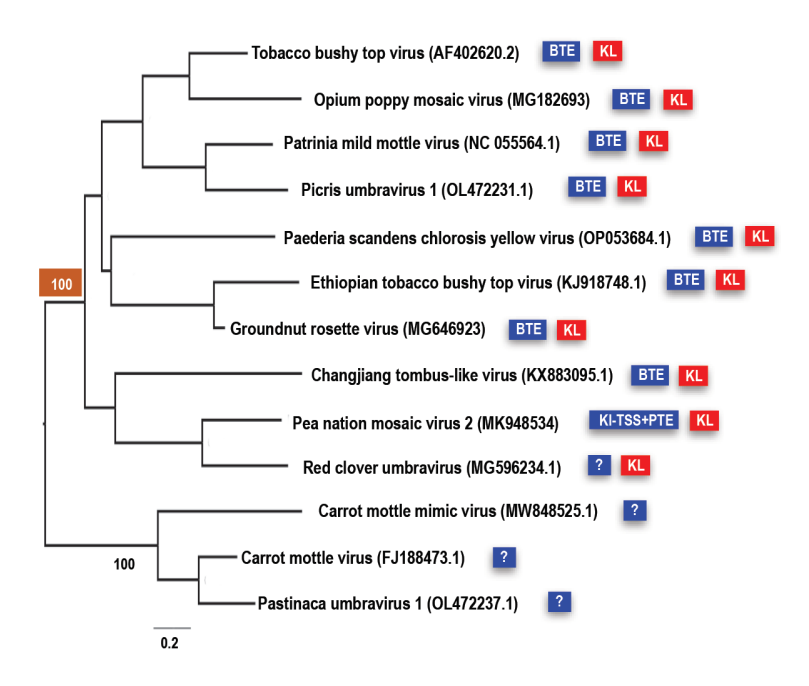


Figure 10. Maximum likelihood phylogenetic tree of umbraviruses based on 3' UTR nucleotide sequences. Values above each branch indicate bootstrap support in the percentage out of 1000 bootstraps. The bottom scale bar indicates nucleotide substitutions per site. The blue and red boxes next to the virus's name indicate the presence of CITE and the KL element, respectively. The bootstrap support for the branch containing closely related umbraviruses possessing the conserved KL element is highlighted in brown.

of the 3'CITE supporting stem (Figures 2 and 3). Umbraviruses without identified 3'CITEs in this central location (CMoMV, CMoV, PasUV1, and RCUV) are predicted to have similar structured elements atop extended stems just downstream of their CAS that likely constitute novel classes of 3'CITEs deserving further attention. The positioning of putative 3'CITEs on extended stems may be advantageous for connecting the CITE to the 5' end by long-distance RNA:RNA interactions, which are required for translation enhancer activity.

Eleven of 14 CAS have an additional element 0 to 1 nt upstream from conserved CAS flanking sequence, which consists of simple hairpins SLX and SLY with apical loops connected by a putative KL of 3 to 5 residues (Figure 1C). Unlike CAS, there is no conservation of sequences among all elements, although several KL contain the common umbravirus and carmovirus tertiary interaction sequence "GCCA"/"UGGC". In addition, umbraviruses that are more closely related, e.g., TBTV, OPMV, Changjiang3, PEMV2, and RCUV (Figure 10) have similar or identical loop sequences with several co-variant residues in the stems and poorly conserved sequence between the hairpins, suggesting a greater importance for maintaining the loop sequence in the KL element. Disruption of the KL interaction in OPMV had no discernable effect on virus accumulation in N. benthamiana cells (Figure 7), suggesting that the KL element in OPMV has a function that does not impact virus accumulation in single cells. While this report identifies the CAS as an important element for umbravirus accumulation, sequences further upstream of the KL element likely also play important roles; as found for umbravirus TBTV, alterations in a sequence upstream of the KL element decreased translation of ORF 1, which correlated with a decrease in viral accumulation and structural changes in BTE apical loops [42].

Many residues in both OPMV and PEMV2 CAS were critical for virus accumulation and altering some of these residues differentially regulated translation of gRNA and

578 579

580

581

582

583

584

585 586 587

593

594595596597598599600

sgRNA reporter constructs. For both OPMV and PEMV2, mutating the conserved apical loop significantly enhanced translation of gRNA but not sgRNA constructs (Figure 5C and Figure 9C), suggesting a conserved function in repressing translation in these umbraviruses. For OPMV, altering or deleting residues in the upper portion of CAS enhanced translation of sgRNA but not gRNA reporter constructs. Disrupting the base of the CAS stem also enhanced translation of the sgRNA, suggesting that CAS has an overall repressive effect on OPMV sgRNA reporter construct translation. In contrast, disrupting the base of the CAS stem reduced translation of the gRNA construct, suggesting that the lower portion of the CAS structure is important for gRNA translation (Figure 5C). The lack of good candidate 5' sequences that might directly interact with unpaired (or paired) OPMV CAS sequences suggests either that CAS may interact indirectly or through non-canonical pairings with 5' sequences or that CAS binds proteins in trans to support functionality. CAS was also critical for PEMV2 accumulation, but unlike OPMV, most mutations in PEMV2 CAS (outside of the apical loop discussed above) had little, if any effect on translation of gRNA or sgRNA reporter constructs. The one exception was deletion of CAS (PmC4), which significantly reduced gRNA reporter levels without affecting sgRNA levels (Figure 9C). Since translation of the reporter constructs was not significantly affected by CAS mutations that reduced or eliminated detectable accumulation in infiltrated plants, it is possible that the PEMV2 reporter constructs were not accurately mimicking translational requirements for the virus.

In addition to clear differences in how CAS affected translation of reporter constructs in the two umbraviruses, WT OPMV and PEMV2 gRNA transcripts differed in whether SHAPE data supported the CAS and KL element structures. For OPMV, the 3'CITE and KL element were well supported, but neither the gRNA nor sgRNA SHAPE profile supported the CAS structure. In contrast, PEMV2 gRNA and sgRNA transcript SHAPE data supported their CAS structures, but not the structures of SLX (gRNA) or SLX and SLY (sgRNA). Since these hairpins are phylogenetically conserved, and since compensatory mutations at the base of the CAS stem restored gRNA levels in vivo for both OPMV (Figure 5B) and PEMV2 (Figure 9B), lack of support for CAS from SHAPE probing of OPMV transcripts could reflect additional RNA conformations in the region, or an unintended consequence of the artificially folded transcripts (i.e., transcripts were not folded co-transcriptionally as would occur in vivo).

Mutations and deletion of OPMV and PEMV2 CAS also differentially affected the RNA structure of regional sequences. For OPMV, few SHAPE reactivity changes were found upstream of CAS whereas the same mutations in PEMV2 CAS significantly affected the structure of the KL element. SHAPE profiles did not reveal any obvious direct interactions between CAS and the adjacent 3'CITEs for either virus, and thus how CAS affects translation remains unknown.

5. Conclusions

Our study identifies the novel, conserved CAS element that is critical for umbravirus accumulation and, with the exception of the apical loop, differentially affects translation of different umbraviruses. A search for hairpins with CAS-conserved features upstream of 3'CITEs in virus members of other genera in the *Tombusviridae* (e.g., BYDV) did not reveal the existence of hairpins with similar conserved features, suggesting that CAS may be uniquely associated with umbraviruses, possibly because of their multiple 3'CITEs. Other hairpins upstream of 3'-proximal CITEs have been found in betanecroviruses TNV-D and beet black scorch virus [26] but their function remains enigmatic. Mutations in one hairpin in TNV-D reduced viral translation in wheat germ extracts but had no effect on accumulation in protoplasts, while similar mutations in a second hairpin reduced accumulation in protoplasts but had no significant effect on in vitro translation. Based on our results and this study, translation of (+)RNA plants viruses is likely far more complex than previously thought.

.

Author Contributions: Conceptualization, SB, MI and AES; SB; formal analysis, SB, MI and AES;
investigation, SB, MI and AAM; resources, AES.; writing—original draft preparation, SB; writing—
review and editing, SB and AES; supervision, AES; project administration, AES; funding acquisition,
AES. All authors have read and agreed to the published version of the manuscript.

Funding: This work was supported by National Science Foundation grants MCB-1411836 and MCB-1818229 to A.E.S.

Institutional Review Board Statement: Not applicable.

Informed Consent Statement: Not applicable. Data Availability Statement: Not applicable.

Acknowledgments: We thank Lwar Naing for his assistance with this work

Conflicts of Interest: The authors declare no conflict of interest.

References

1. Simon, A.E.; Miller, W.A. 3' Cap-independent translation enhancers of plant viruses. Annu. Rev. Microbiol. 2013, 67, 21-

Truniger, V.; Miras, M.; Aranda, M.A. Structural and functional diversity of plant virus 3'-cap-independent translation 2. enhancers (3'-CITEs). Front. Plant Sci. 2017, 8, 1-14.

- Geng, G.; Yu, C.; Li, X.; Yuan, X. A unique internal ribosome entry site representing a dynamic equilibrium state of rna 3. tertiary structure in the 5'-UTR of wheat yellow mosaic virus RNA1. Nucleic Acids Res. 2020, 48, 390-404.
- 4. Jaramillo-Mesa, H.; Gannon, M.; Holshbach, E.; Zhang, J.; Roberts, R.; Buettner, M.; Rakotondrafaraa, A.M. The triticum mosaic virus internal ribosome entry site relies on a picornavirus-like YX-AUG motif to designate the preferred translation initiation site and to likely target the 18S rRNA. J. Virol. 2019, 93, e01705-18.
- Basso, J.; Dallaire, L.P.; Charest, P.J.; Devantier, Y.; Laliberte, J.F. Evidence for an internal ribosome entry site within the 5. 5' non-translated region of turnip mosaic potyvirus RNA. J. Gen. Virol. 1994, 75, 3157–3165.
- 6. May, J.; Johnson, P.; Saleem, H.; Simon, A.E. A Sequence-independent, unstructured internal ribosome entry site is responsible for internal expression of the coat protein of turnip crinkle virus. J. Virol. 2017, 91, 1–16.
- Wang, J.; Zhang, X.; Greene, G.H.; Xu, G.; Wang, J.; Zhang, X.; Greene, G.H.; Xu, G.; Dong, X. PABP/purine-rich motif 7. as an initiation module for cap-independent translation in pattern-triggered immunity. Cell 2022, 185, 1-15.
- Ilyas, M.; Du, Z.; Simon, A.E. Opium poppy mosaic virus has an Xrn-resistant, translated subgenomic rna and a BTE 3' 8. 694 CITE. J. Virol. 2021, 95, 1-21.
- 9. Gao, F.; Kasprzak, W.K.; Szarko, C.; Shapiro, B.A.; Simon, A.E. The 3' untranslated region of pea enation mosaic virus contains two T-shaped, ribosome-binding, cap-independent translation enhancers. J. Virol. 2014, 88, 11696–11712.
- 10. Du, Z.; Alekhina, O.M.; Vassilenko, K.S.; Simon, A.E. Concerted action of two 3' cap-independent translation enhancers increases the competitive strength of translated viral genomes. Nucleic Acids Res. 2017, 45, 9558–9572.
- Weingarten-Gabbay, S.; Elias-Kirma, S.; Nir, R.; Gritsenko, A.A.; Stern-Ginossar, N.; Yakhini, Z.; Weinberger, A.; Segal, 11. E. Comparative genetics: systematic discovery of cap-independent translation sequences in human and viral genomes. Science. 2016, 351(6270):aad4939.
- 12. Nieto, C.; Rodríguez-Moreno, L.; Rodríguez-Hernández, A.M.; Aranda, M.A.; Truniger, V. Nicotiana benthamiana resistance to non-adapted melon necrotic spot virus results from an incompatible interaction between virus rna and translation initiation factor 4E. Plant J. 2011, 66, 492-501.
- 13. Truniger, V.; Nieto, C.; González-Ibeas, D.; Aranda, M. Mechanism of Plant EIF4E-Mediated Resistance against a Carmovirus (Tombusviridae): Cap-independent translation of a viral RNA controlled in cis by a virulence determinant. Plant J. 2008, 56, 716-727.
- 14. Miras, M.; Sempere, R.N.; Kraft, J.J.; Miller, W.A.; Aranda, M.A.; Truniger, V. Interfamilial recombination between viruses

676 677

670

671

672

673

674

675

678 679

681 682

683

680

684 685

> 686 687

688

689 690

692

693

695

696

697

698

699

700

701

702

703

704 705

706 707

708

- led to acquisition of a novel translation-enhancing RNA element that allows resistance breaking. *New Phytol.* **2014**, *202*, 233–246.
- 15. Treder, K.; Pettit Kneller, E.L.; Allen, E.M.; Wang, Z.; Browning, K.S.; Miller, W.A. The 3' cap-independent translation element of barley yellow dwarf virus binds eIF4F via the eIF4G subunit to initiate translation. *RNA* **2008**, *14*, 134–147.
- Wang, Z.; Treder, K.; Miller, W.A. Structure of a viral cap-independent translation element that functions via high affinity
 binding to the eIF4E Subunit of eIF4F. J. Biol. Chem. 2009, 284, 14189–14202.
- 17. Johnson, P.Z.; Kasprzak, W.K.; Shapiro, B.A.; Simon, A.E. Structural characterization of a new subclass of panicum mosaic virus-like 3' cap-independent translation enhancer. *Nucleic Acids Res.* **2022**, *50*, 1601–1619.
- 18. Zuo, X.; Wang, J.; Yu, P.; Eyler, D.; Xu, H.; Starich, M.R.; Tiede, D.M.; Simon, A.E.; Kasprzak, W.; Schwieters, C.D.; et al. Solution structure of the cap-independent translational enhancer and ribosome-binding element in the 3' UTR of turnip crinkle virus. *Proc. Natl. Acad. Sci. U. S. A.* **2010**, *107*, 1385–1390.
- 19. Wang, Z.; Parisien, M.; Scheets, K.; Miller, W.A. The cap-binding translation initiation factor, eIF4E, binds a pseudoknot in a viral cap-independent translation element. *Structure* **2011**, *19*, 868–880.
- 20. Chattopadhyay, M.; Shi, K.; Yuan, X.; Simon, A.E. Long-distance kissing loop interactions between a 3' proximal Y-shaped structure and apical loops of 5' hairpins enhance translation of saguaro cactus virus. *Virology* **2011**, *417*, 113–125.
- 21. Gao, F.; Simon, A.E. Differential use of 3'CITEs by the subgenomic rna of pea enation mosaic virus 2. *Virology* **2017**, *510*, 194–204.
- 22. McCormack, J.C.; Yuan, X.; Yingling, Y.G.; Kasprzak, W.; Zamora, R.E.; Shapiro, B.A.; Simon, A.E. Structural domains within the 3' untranslated region of turnip crinkle virus. *J. Virol.* **2008**, *82*, 8706–8720.
- 23. Stupina, V.A.; Meskauskas, A.; Mccormack, J.C.; Yingling, Y.G.; Shapiro, B.A.; Dinman, J.D.; Simon, A.E. The 3' proximal translational enhancer of turnip crinkle virus binds to 60S ribosomal subunits. *RNA* **2008**, *14*, 2379–2393.
- 24. Le, M.T.; Kasprzak, W.K.; Kim, T.; Gao, F.; Young, M.Y.L.; Yuan, X.; Shapiro, B.A.; Seog, J.; Simon, A.E. Folding behavior of a T-shaped, ribosome-binding translation enhancer implicated in a wide-spread conformational switch. *eLife* **2017**, *6*, 1–24.
- 25. Yuan, X.; Shi, K.; Simon, A.E. A Local, Interactive network of 3' RNA elements supports translation and replication of turnip crinkle virus. *J. Virol.* **2012**, *86*, 4065–4081.
- 26. Newburn, L.R.; Wu, B.; Andrew White, K. Investigation of novel RNA elements in the 3'UTR of tobacco necrosis virus-D. *Viruses* **2020**, *12*, 1–12.
- 27. Iwakawa, H.; Tajima, Y.; Taniguchi, T.; Kaido, M.; Mise, K.; Tomari, Y.; Taniguchi, H.; Okuno, T. Poly(A)-binding protein facilitates translation of an uncapped/nonpolyadenylated viral RNA by binding to the 3' untranslated region. *J. Virol.* **2012**, *86*, 7836–7849.
- 28. Yuan, X.; Shi, K.; Meskauskas, A.; Simon, A.E. The 3' end of turnip crinkle virus contains a highly interactive structure including a translational enhancer that is disrupted by binding to the RNA-dependent RNA polymerase. *RNA* **2009**, *15*, 1849–1864.
- 29. Ryabov, E.; Taliansky, M.E.; Robinson, D.; Waterhouse, P.; Murant, A.F.; de Zoeten, G.; Falk, B.; Vetten, H.; Gibbs, M. Genus Umbravirus. In: King, A. M. Q., Adams, M.J., Carstens, E., & Lefkowitz, E. J. (Eds.) Virus Taxonomy: Ninth Report of the International Committee on Taxonomy of Viruses. *Elsevier Sci.* 2012, 1191–1195.
- 30. May, J.P.; Yuan, X.; Sawicki, E.; Simon, A.E. RNA virus evasion of nonsense-mediated decay. *PLoS Pathog.* **2018**, *14*, 1–747
- 31. Gao, F.; Alekhina, O.M.; Vassilenko, K.S.; Simon, A.E. Unusual dicistronic expression from closely spaced initiation codons in an umbravirus subgenomic RNA. *Nucleic Acids Res.* **2018**, *46*, 11726–11742.
- 32. Bera, S.; Blundell, R.; Liang, D.; Crowder, D.W.; Casteel, C.L. The oxylipin signaling pathway is required for increased

- aphid attraction and retention on virus-infected plants. J. Chem. Ecol. 2020, 46, 771–781.
- 33. May, J.P.; Johnson, P.Z.; Ilyas, M.; Gao, F.; Simon, E. The multifunctional long-distance movement protein of pea enation mosaic virus 2 protects viral and host transcripts from nonsense-mediated decay. *MBio* **2020**, *11*, 1–16.
- 34. Gao, F.; Gulay, S.P.; Kasprzak, W.; Dinman, J.D.; Shapiro, B.A.; Simon, A.E. The kissing-loop T-shaped structure translational enhancer of pea enation mosaic virus can bind simultaneously to ribosomes and a 5' proximal hairpin. *J. Virol.* **2013**, *87*, 11987-12002.
- 35. Gao, F.; Kasprzak, W.; Stupina, V.A.; Shapiro, B.A.; Simon, A.E. A ribosome-binding, 3' translational enhancer has a T-shaped structure and engages in a long-distance RNA-RNA interaction. *J. Virol.* **2012**, *86*, 9828–9842.
- 36. Liu, H.; Naismith, J.H. An efficient one-step site-directed deletion, insertion, single and multiple-site plasmid mutagenesis protocol. *BMC Biotechnol.* **2008**, *8*, 91.
- 37. Wilkinson, K.A.; Merino, E.J.; Weeks, K.M. Selective 2'-Hydroxyl Acylation Analyzed by Primer Extension (SHAPE): Quantitative RNA structure analysis at single nucleotide resolution. *Nat. Protoc.* **2006**, *1*, 1610–1616.
- 38. Liu, J.; Carino, E.; Bera, S.; Gao, F.; May, J.P.; Simon, A.E. Structural analysis and whole genome mapping of a new type of plant virus subviral RNA: umbravirus-like associated RNAs. *Viruses* **2021**, *13*.
- 39. Zuker, M. Mfold Web Server for Nucleic Acid Folding and Hybridization Prediction. *Nucleic Acids Res.* **2003**, *31*, 3406–3415.
- 40. Karabiber, F.; McGinnis, J.L.; Favorov, O. V.; Weeks, K.M. QuShape: Rapid, accurate, and best-practices quantification of nucleic acid probing information, resolved by capillary electrophoresis. *RNA* **2013**, *19*, 63–73.
- 41. Johnson, P.Z.; Kasprzak, W.K.; Shapiro, B.A.; Simon, A.E. RNA2Drawer: Geometrically strict drawing of nucleic acid structures with graphical structure editing and highlighting of complementary subsequences. *RNA Biol.* **2019**, *16*, 1667–1671.
- 42. Wang, D.; Yu, C.; Liu, S.; Wang, G.; Shi, K.; Li, X.; Yuan, X. Structural alteration of a BYDV-like translation element (BTE) that attenuates p35 expression in three mild tobacco bushy top virus isolates. *Sci. Rep.* **2017**, 7, 1–10.